PROBLEMY MECHATRONIKI
UZBROJENIE, LOTNICTWO, INŻYNIERIA BEZPIECZEŃSTWA

ISSN 2081-5891

9, 4 (34), 2018, 127-148

PROBLEMS OF MECHATRONICS
ARMAMENT, AVIATION, SAFETY ENGINEERING

Vibrations and Stability of a Plate in Supersonic Flow Subjected to a Follower Force, and Having a Hinged External Support and a Resilient Attenuation Internal Support

Idzi NOWOTARSKI

Military University of Technology, Faculty of Mechatronics and Aerospace,
2 gen. Witolda Urbanowicza Str., 00-908 Warsaw, Poland
E-mail address: idzi.nowotarski@wat.edu.pl

Received by the editorial staff on 4 December 2016
The reviewed and verified version was received on 28 December 2018

DOI 10.5604/01.3001.0012.7338

Abstract. The vibrations and stability of a plate having a finite length were considered in a flat supersonic flow, having adopted an assumption that one of the edges of the plate has a hinged support, and the other edge is free. Another support was located in an internal point of the plate and featured resilient attenuation properties. A compressive force, called the follower force, was applied within the plane of the plate in a direction tangent to the deformed surface of the plate. This way, a superficial system was forced in which two independent physical factors occurred and caused its self-excitation. Therefore the superficial system could be termed a 'double self-excited system'. The solution of the equations of motion for the system was derived with a Laplace transformation.

In the further part of the work, a numerical analysis was carried out for the conditions of the occurrence of self-excited vibrations in relation to the position of the internal support (the so-called plate overhang), the damping within the material of the plate and other parameters of the plate, including the resilient attenuation parameters of the internal support. For the adopted parameters, the results were tested for the calculations of the stability area limits and the instability of the system in plane γ_1, σ. The forms of vibrations for a series of typical cases was determined.
Keywords: mechanics, aeroelasticity, computer calculations

1. FORMULATION OF THE PROBLEM

The vibrations and stability of superficial systems exposed to supersonic flow conditions have been investigated in a number of scientific papers (see e.g. [1], [2], [5] and the references therein). The effect of follower forces on the stability of superficial systems was investigated in [3] and [6] to [9], whereas the vibrations and stability of bracket plates exposed to supersonic flow conditions and a follower force was researched in [4].

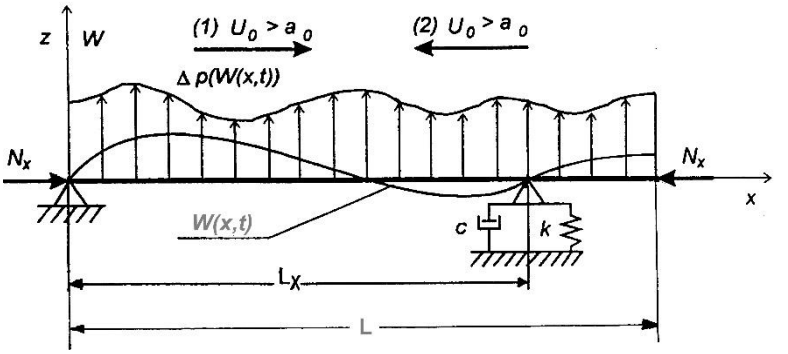

Fig. 1.1. Model of a plate in a supersonic flow subject to the application of a follower force applied and equipped with an internal resilient attenuation support

In this paper, which is an expanded analysis of the problem detailed in [9], necessitated by different conditions of support, a plate of a finite length L was investigated being exposed to single-sided flat supersonic flow at a velocity of $U_0 > a_0$ (Fig. 1.1), with a_0 being the speed of sound.

The left-hand edge of the plate was supported with a hinge; the other, inner edge of the plate featured a resilient support with a rigidity of k and an attenuation coefficient of c. The right-hand edge of the plate was free. Two directions of supersonic flow at a velocity of U_0 were investigated as shown in Fig. 1, in case *(1)* and *(2)*.

The equation of motion of the plate was shown in the forms [1], [2], [4], and [9]:

$$D\left(1+\theta\frac{\partial}{\partial t}\right)\frac{\partial^4 W}{\partial x^2}+N_0\frac{\partial^2 W}{\partial x^2}+\rho_p h\frac{\partial^2 W}{\partial t^2}=\Delta p_{1,2}\left(W(x,t)\right) \tag{1.1}$$

with:

$$\Delta p_{1,2}\left(W(x,t)\right)=-\frac{\rho_o U_o}{\mu}\left[(1-\frac{1}{\mu^2})\frac{\partial W}{\partial x}\pm U_o\frac{\partial W}{\partial x}\right] \tag{1.2}$$

– differential pressure applied to the plate in case *(1)* with the sense (+) or, as shown in case *(2)* with the sense (-) preceding the second term in (1.2):

$$D\left(1+\theta\frac{\partial}{\partial t}\right)\frac{\partial^4 W}{\partial x^2}+N_0\frac{\partial^2 W}{\partial x^2}+\rho_p h\frac{\partial^2 W}{\partial t^2}=\Delta p_{1,2}\left(W(x,t)\right) \tag{1.3}$$

D – bending rigidity of the panel; Θ – material attenuation coefficient, per the Voigt model; ρ_p – material density of the plate; h – thickness of the plate; ρ_0 – gas density in a non-turbulent flux; M – Mach number of the gas flow.

For the left-hand edge of the plate, given $x = 0$, the boundary conditions were assumed as follows for the case of the hinge-supported edge:

$$W(0,t)=\left.\frac{\partial^2 W(x,t)}{\partial x^2}\right|_{x=0}=0 \tag{1.4}$$

For the right-hand free edge of the plate, with $x = L$, the following boundary conditions were assumed:

$$\left.\frac{\partial^2 W(x,t)}{\partial x^2}\right|_{x=L}=\left.\frac{\partial^3 W(x,t)}{\partial x^3}\right|_{x=L}=0 \tag{1.5}$$

At the inner point of interval (0, L), where the resilient attenuation inner support was located, two geometric conditions had to be satisfied, where one of them was imposed from the continuity of deflection:

$$W(L_x-0,t)=W(L_x+0,t)=0 \tag{1.6}$$

the other was imposed by the continuity of deflection angles:

$$\left.\frac{\partial W(x,t)}{\partial x}\right|_{x=L_x-0}=\left.\frac{\partial W(x,t)}{\partial x}\right|_{x=L_x+0}=0 \tag{1.7}$$

Further conditions which needed to be satisfied for $x = L_x$, were two static equilibrium conditions in the following forms:

$$\left.\frac{\partial^2 W(x,t)}{\partial x^2}\right|_{x=L_x-0} = \left.\frac{\partial^2 W(x,t)}{\partial x^2}\right|_{x=L_x+0} = 0 \tag{1.8}$$

$$D\left(1+\theta_r \frac{\partial}{\partial t}\right)\left.\frac{\partial^3 W(x,t)}{\partial x^3}\right|_{x=L_x-0} - D\left(1+\theta_r \frac{\partial}{\partial t}\right)\left.\frac{\partial^3 W(x,t)}{\partial x^3}\right|_{x=L_x+0} = = k\,W(L_x-0,t)+c\frac{\partial W(L_x-0,t)}{\partial t} \tag{1.9}$$

The problem was investigated as a dimensionless one, with the assumption that displacements W and coordinate x referred to the plate length, L, i.e. $\xi = x/L$, whereas time t referred to $1/\omega_1$, i.e. $\tau = t\,\omega_1$, with:

$$\omega_1 = \sqrt{\frac{D}{\rho_p h}} \tag{1.10}$$

– basic natural vibration frequency of the plate with the fixed hinged support in a vacuum at $N_0 = \Theta = 0$.
Hence, equation (1.1) was as follows with dependence (1.2):

$$\left(1+\theta_r \frac{\partial}{\partial \tau}\right)\frac{\partial^4 W(\xi,\tau)}{\partial \xi^4} + S_0 \frac{\partial^2 W(\xi,\tau)}{\partial \xi^2} + \gamma_1 \frac{\partial W(\xi,\tau)}{\partial \xi} + + \pi^4 \frac{\partial^2 W(\xi,\tau)}{\partial \tau^2} + \gamma_2 \frac{\partial W(\xi,\tau)}{\partial \tau} = 0 \tag{1.11}$$

with:

$$\omega_r = \theta\,\omega_1,\ S_0 = \frac{N_0 L^2}{D},\ \gamma_1 = \pm\frac{\rho_0 U_0^2 L^3}{\mu D},\ \gamma_2 = |\gamma_1|\,\delta, \quad \delta = \frac{L\omega_1}{a_0 M}\left(1-\frac{1}{\mu^2}\right) \tag{1.12}$$

The formula of γ_1 had the sense (+) or (-), respective to the direction of flow, not unlike in equation (1.2). Boundary conditions (1.4) to (1.9) for dimensionless coordinates (+) were formulated as follows:

$$W(0,\tau) = \left.\frac{\partial^2 W(\xi,\tau)}{\partial \xi^2}\right|_{\xi=0} = 0 \tag{1.13}$$

$$\left.\frac{\partial^2 W(\xi,\tau)}{\partial \xi^2}\right|_{\xi=1} = \left.\frac{\partial^3 W(\xi,\tau)}{\partial \xi^3}\right|_{\xi=1} = 0 \tag{1.14}$$

For the internal point of interval (0, 1):

$$W(\xi_x - 0, \tau) = W(\xi_x + 0, \tau) = 0 \tag{1.15}$$

$$\left.\frac{\partial W(\xi,\tau)}{\partial \xi}\right|_{\xi=\xi_x-0} = \left.\frac{\partial W(\xi,\tau)}{\partial \xi}\right|_{\xi=\xi_x+0} = 0 \tag{1.16}$$

$$\left.\frac{\partial^2 W(\xi,\tau)}{\partial \xi^2}\right|_{\xi=\xi_x-0} = \left.\frac{\partial^2 W(\xi,\tau)}{\partial \xi^2}\right|_{\xi=\xi_x+0} = 0 \tag{1.17}$$

$$\left(1+\theta_r\frac{\partial}{\partial\tau}\right)\left.\frac{\partial^3 W(\xi,\tau)}{\partial \xi^3}\right|_{\xi=\xi_x-0} - \left(1+\theta_r\frac{\partial}{\partial\tau}\right)\left.\frac{\partial^3 W(\xi,\tau)}{\partial \xi^3}\right|_{\xi=\xi_x+0} = k_r W(\xi_x - 0, \tau) + c_r \frac{\partial W(\xi_x - 0, \tau)}{\partial \tau} \tag{1.18}$$

with:

$$\xi_x = \frac{L_x}{L},\ 0 << \xi_x < 1,\ k_r = \frac{k L^3}{D},\ c_r = \frac{c L^3 \omega_1}{D} \tag{1.19}$$

Equation (1.11) featured two dimensionless parameters, S_0 and γ_1, which could trigger self-excitation of the system. This is why the system was termed a 'double self-excited system'.

2. SOLUTION OF THE PROBLEM

Given the discontinuity of the parameters within interval (0, 1), i.e. $\xi = \xi_x$ the solution to equation (1.11) was sought in the following form:

$$W(\xi,\tau) = \begin{cases} W_1(\xi,\tau) = V_1(\xi)e^{ip\tau} & \text{for} \quad 0 \le \xi \le \xi_x \\ W_2(\xi,\tau) = \left[V_1(\xi) + V_2(\xi - \xi_x)\right]e^{ip\tau} & \text{for} \quad \xi_x \le \xi \le 1 \end{cases} \tag{2.1}$$

where function $W_j(\xi)$ satisfied this equation

$$(1 + ip\theta_r)W_j''''(\xi) + S_0 W_j''(\xi) + \gamma_1 W_j'(\xi) + \left(i\gamma_2 p - \pi^4 p^2\right)W_j(\xi) = 0, \quad j = 1, 2 \tag{2.2}$$

For the first interval ($0 \le \xi \le \xi_x$), the application of the Laplace transformation expressed as

$$\overline{V_1}(s) = \mathrm{L}\, V_1(\xi) = \int_0^\infty e^{-s\xi} V_1(\xi)\, d\xi \tag{2.3}$$

to equation (2.2), the solution in the image domain had the form of

$$\begin{aligned}\overline{V}_1(s)\left(s^4+b_2s^2+b_1s+b_0\right)=V_1(0)\left(s^2+b_2s+b_1\right)+\\+V_1'(0)\left(s^2+b_2\right)+V_1''(0)s+V_1'''(0)\end{aligned} \tag{2.4}$$

with $V_1(0), V_1'(0), V_1''(0), V_1'''(0)$ as the original values of function $V_1(\xi)$ and its derivatives, whereas the substituted coefficients b_j described these dependences

$$b_0=\frac{i\gamma_2 p-\pi^4 p^2}{1+ip\theta_r},\quad b_1=\frac{\gamma_1}{1+ip\theta_r},\quad b_2=\frac{S_0}{1+ip\theta_r}, \tag{2.5}$$

Further on, the use of the denotations

$$\upsilon_{10}=V_1(0)=0,\quad \upsilon_{11}=V_1'(0),\quad \upsilon_{12}=V_1''(0)=0,\quad \upsilon_{13}=V_1'''(0) \tag{2.6}$$

and equation (2.4) in a form convenient for further operations was

$$\begin{aligned}\overline{V}_1(s)=\frac{s^2+b_2s+b_1}{s^4+b_2s^2+b_1s+b_0}\upsilon_{10}+\frac{s^2+b_2}{s^4+b_2s^2+b_1s+b_0}\upsilon_{11}+\\+\frac{s}{s^4+b_2s^2+b_1s+b_0}\upsilon_{12}+\frac{1}{s^4+b_2s^2+b_1s+b_0}\upsilon_{13}\end{aligned} \tag{2.7}$$

The inverse Laplace transform applied to equation (2.7), and given boundary conditions (2.6), the result was

$$V_1(\xi)=\left[K''(\xi)+b_2K(\xi)\right]\upsilon_{11}+K(\xi)\upsilon_{13} \tag{2.8}$$

The theorem of original differentiation for the second interval, i.e. ($\xi_x \le \xi \le 1$) could not be applied to the function present in that interval with an offset of $V_2(\xi-\xi_x)$, since the function was differentiable at point $\xi=\xi_x$. This restriction was correct if derivative $V_2'(\xi-\xi_x)$ was determined in classical analytical terms, like in [10]. However, with the following assumption

$$V_2'(\xi-\xi_x)=\delta(\xi-\xi_x) \tag{2.9}$$

the rule could be applied, because

$$\mathrm{L}\left[V_2'(\xi-\xi_x)\right]=s\mathrm{L}\left[V_2(\xi-\xi_x)\right]-V_2(-\xi_x) \tag{2.10}$$

Detailed contemplations of the Laplace transformation into the function with an offset can be found in [10], which is dedicated fully to the practical applications of the Laplace transformation.

Having reached the foregoing notes, for the second interval (see eq. (2.1)), equation (2.2) in the original space and given the used denotations (2.5) was

$$\begin{aligned}V_1'''(\xi)+V_2''''(\xi-\xi_x)+b_2\left[V_1''(\xi)+V_2''(\xi-\xi_x)\right]+\\+b_1\left[V_1'(\xi)+V_2'(\xi-\xi_x)\right]+b_0\left[W_1(\xi)+W_1(\xi-\xi_x)\right]=0\end{aligned} \tag{2.11}$$

which, following the Laplace transformation, i.e. the transition from the original space to the image space, led to this expression

$$\begin{aligned}&\mathsf{L}\left[V_2(\xi-\xi_x)\right]\left(s^4+b_2s^2+b_1s+b_0\right)=-\mathsf{L}\left[V_1(\xi)\right]\left(s^4+b_2s^2+b_1s+b_0\right)+\\&+\left(s^3+b_2s+b_1\right)V_1(0)+\left(s^2+b_2\right)V_1'(0)+sV_1''(0)+V_1'''(0)+\\&+\left(s^3+b_2s+b_1\right)V_2(-\xi_x)+\left(s^2+b_2\right)V_2'(-\xi_x)+sV_2''(-\xi_x)+V_2'''(-\xi_x)\end{aligned}\tag{2.12}$$

With the conventional denotations from (2.6), i.e. the first subscript denoted the integration range and the second subscript denoted the order of the derivative, the following was obtained in the second interval:

$$\upsilon_{20}=V_2(-\xi_x),\quad \upsilon_{21}=V_2'(-\xi_x),\quad \upsilon_{22}=V_2''(-\xi_x),\quad \upsilon_{23}=V_2'''(-\xi_x)\tag{2.13}$$

The inverse Laplace transform on equation (2.12) with the boundary conditions of (2.6) and (2.13), and with the necessary transformations, defined the sought displacement function $V_2(\xi-\xi_a)$

$$\begin{aligned}V_2(\xi-\xi_x)=&\left[K'''(\xi)+b_2K'(\xi)+b_1K(\xi)\right]\upsilon_{20}+\left[K''(\xi)+b_2K(\xi-\xi_x)\right]\upsilon_{21}+\\&+K'(\xi)\upsilon_{22}+K(\xi)\upsilon_{23}\end{aligned}\tag{2.14}$$

The unknown coefficients v_{ij} present in equations (2.8) and (2.14) were determined with the geometric boundary conditions of (1.15) and (1.16), and the static boundary conditions of (1.14), (1.17), and (1.18), which assumed the following form when substituted to (2.1):

$$V_2''(1)=V_2'''(1)=0\tag{2.15}$$

$$V_1(\xi_x)=V_2(\xi_x)\tag{2.16}$$

$$V_1'(\xi_x)=V_2'(\xi_x)\tag{2.17}$$

$$V_1''(\xi_x)=V_2''(\xi_x)\tag{2.18}$$

$$\left(1+\theta_r ip\right)\left[V_1'''(\xi_x)-V_2'''(\xi_x)\right]=\left(k_r+c_r ip\right)V_1(\xi_x)\tag{2.19}$$

Function K(ξ) in equations (2.8) and (2.14) was determined in the following form

$$K(\xi)=\sum_{j=1}^{4}c_j\exp\left(s_j\,\xi\right)\tag{2.20}$$

with s_j being the radicals of the characteristic equation (see (2.4))

$$d(s)=s^4+b_2s^2+b_1s+b_0=0\tag{2.21}$$

whereas coefficients c_j were expressed as

$$c_j = \frac{1}{d'(s_j)} = \frac{1}{4s_j^3 + 2b_2 s_j + b_1}, \quad j = 1,2,3,4. \tag{2.22}$$

With the originals of function $V_j(\xi)$ known as described with equations (2.8) and (2.14), the boundary conditions of (2.15) to (2.19) provided the following matrix system of uniform equations

$$\underset{(6\times6)}{\mathbf{W}} \cdot \underset{(6\times1)}{\boldsymbol{\upsilon}} = \underset{(6\times1)}{\mathbf{0}} \tag{2.23}$$

with vector υ having these components

$$\boldsymbol{\upsilon}^T = \begin{bmatrix} \upsilon_{11} & \upsilon_{13} & \upsilon_{20} & \upsilon_{21} & \upsilon_{22} & \upsilon_{23} \end{bmatrix} \tag{2.24}$$

whereas the matrix elements w were

$$\left.\begin{aligned}
&w_{11} = K^{(IV)}(1) + b_2 K''(1), \quad w_{12} = K''(1), \quad w_{13} = K^{(V)}(1) + b_1 K''(1) + b_2 K'''(1),\\
&w_{14} = K^{(IV)}(1) + b_2 K''(1), \quad w_{15} = K'''(1), \quad w_{16} = K''(1),\\
&w_{21} = K^{(V)}(1) + b_2 K'''(1), \quad w_{22} = K'''(1), \quad w_{23} = K^{(VI)}(1) + b_1 K'''(1) + b_2 K^{(IV)}(1),\\
&w_{24} = K^{(V)}(1) + b_2 K'''(1), \quad w_{25} = K^{(IV)}(1), \quad w_{26} = K'''(1),\\
&w_{31} = 0, \quad w_{32} = 0, \quad w_{33} = -K'''(\xi_x) - b_1 K(\xi_x) - b_2 K'(\xi_x),\\
&w_{34} = -K''(\xi_x) - b_2 K(\xi_x), \quad w_{35} = -K'(\xi_x), \quad w_{36} = -K(\xi_x),\\
&w_{41} = 0, \quad w_{42} = 0, \quad w_{43} = -K^{(IV)}(\xi_x) - b_1 K'(\xi_x) - b_2 K''(\xi_x),\\
&w_{44} = -K'''(\xi_x) - b_2 K'(\xi_x), \quad w_{45} = -K''(\xi_x), \quad w_{46} = -K'(\xi_x),\\
&w_{51} = 0, \quad w_{52} = 0, \quad w_{53} = -K^{(V)}(\xi_x) - b_1 K''(\xi_x) - b_2 K'''(\xi_x),\\
&w_{54} = -K^{(IV)}(\xi_x) - b_2 K''(\xi_x), \quad w_{55} = -K'''(\xi_x), \quad w_{56} = -K''(\xi_x),\\
&w_{61} = (1 + i\Theta_r p)\left[K^{(V)}(\xi_x) + b_2 K'''(\xi_x)\right] - (k_r + ic_r p)\left[K''(\xi_x) + b_2 K(\xi_x)\right] +\\
&\quad - b_2 K(\xi_x) - K''(\xi_x)\\
&w_{62} = (1 + i\Theta_r p)K'''(\xi_x) - (k_r + ic_r p)K(\xi_x) - K(\xi_x),\\
&w_{63} = -K'''(\xi_x) - b_1 K(\xi_x) - b_2 K'(\xi_x), \qquad w_{64} = -K''(\xi_x) + b_2 K(\xi_x),\\
&w_{65} = -K'(\xi_x), \qquad w_{66} = -K(\xi_x)
\end{aligned}\right\} \tag{2.25}$$

The solution which presented the steady-state vibrations of the system could be expressed as follows:

$$W(\xi,\tau) = \mathrm{Re}\begin{cases} W_1(\xi,\tau) = a_1(\xi)\cos\left(p\tau + \varphi_1(\xi)\right) & \text{dla} \quad 0 \le \xi \le \xi_x \\ W_2(\xi,\tau) = a_2(\xi)\cos\left(p\tau + \varphi_2(\xi)\right) & \text{dla} \quad \xi_x \le \xi \le 1 \end{cases} \tag{2.26}$$

with:

$$\left.\begin{aligned} a_j(\xi) &= \sqrt{\left(\mathrm{Re}\,W_j(\xi)\right)^2 + \left(\mathrm{Im}\,W_j(\xi)\right)^2} \\ tg\varphi_j(\xi) &= \frac{\mathrm{Im}\,W_j(\xi)}{\mathrm{Re}\,W_j(\xi)} \end{aligned}\right\}, \quad j = 1,2 \tag{2.27}$$

The frequency equation expressed from the system of uniform equations in (2.23), i.e.

$$\Delta = \det(\mathbf{w}) = 0 \tag{2.28}$$

was applied to analyse the stability and vibrations of the investigated system.

3. NUMERICAL ANALYSIS OF SELF-EXCITED VIBRATIONS

The trend of the critical parameters of self-excited vibrations was investigated in relation to the plate overhang dimensionless parameter value of $\xi_x = L_x/L$ and a number of other data items. The frequency equation of (2.28) was applied to analyse the stability and vibrations of the investigated system. In a general case, vibrational frequency p was assumed to be complex:

$$p = q - i\varepsilon, \tag{3.1}$$

this facilitated the following general expression:

$$\Delta = \mathrm{Re}\,\Delta + i\,\mathrm{Im}\,\Delta = 0, \tag{3.2}$$

For the given values of S_0, γ_1, γ_2, Θ_r, k_r, c_r, ξ_x, the frequency equations of (3.2) facilitated the determination of the system's natural vibration frequency $q = q_n$, $n = 1, 2, \ldots$ and the decay decrements $\varepsilon = \varepsilon_n < 0$ (for attenuated vibrations) or the decrements of increase $\varepsilon = \varepsilon_n > 0$ (for unstable self-excited vibrations). The frequency vibrations also facilitated the determination of the critical parameters of self-excited vibrations of the system, S_{okr}, q_{kr}, at $\varepsilon = 0$ and the given γ_1, γ_2, Θ_r, k_r, c_r, ξ_x, or γ_{1kr}, q_{kr} at $\varepsilon = 0$ and the assumed S_0, γ_2, Θ_r, k_r, c_r, ξ_x, with S_{okr} and γ_{1kr} were the smallest values of S_0 and γ_1 that occurred at the vibration stability limit, whereas q_{kr} was the vibration frequency for which $\varepsilon = 0$ at $S_0 = S_{0kr}$ or $\gamma_1 = \gamma_{1kr}$.

If $q = \varepsilon = 0$, then for the assumed values of all other parameters in the frequency equations, the divergent stability loss limits could be determined as the values of S_{okr} and γ_{1kr}.

3.1. Determination of the critical parameters of the plate on a fixed hinged support with a small overhang ($\xi_x = 0.9$)

The critical parameters were determined for the investigated case by testing the trends of the solutions to equation (2.28) in the vicinity of the few first natural vibration frequencies of the system, and at these frequencies, self-excited vibrations would usually occur. Solving equation (2.28) divided into the real part and the imaginary part (3.2) for harmonic vibrations ($\varepsilon = 0$) and non-stationary vibrations ($\varepsilon \neq 0$) in dependence of S_0, γ_1, δ Θ_r and k_r, c_r, plane $\gamma_1 - q$ featured the plots of roots of equations (3.2), the examples of which, given $\varepsilon = 0$, are shown in Fig. 3.1 at $\sigma = 0$ and in Fig. 3.2 at $\sigma = 2$. The parameter input σ was described with the following dependence:

$$\sigma = S_0 / \pi^2 \tag{3.3}$$

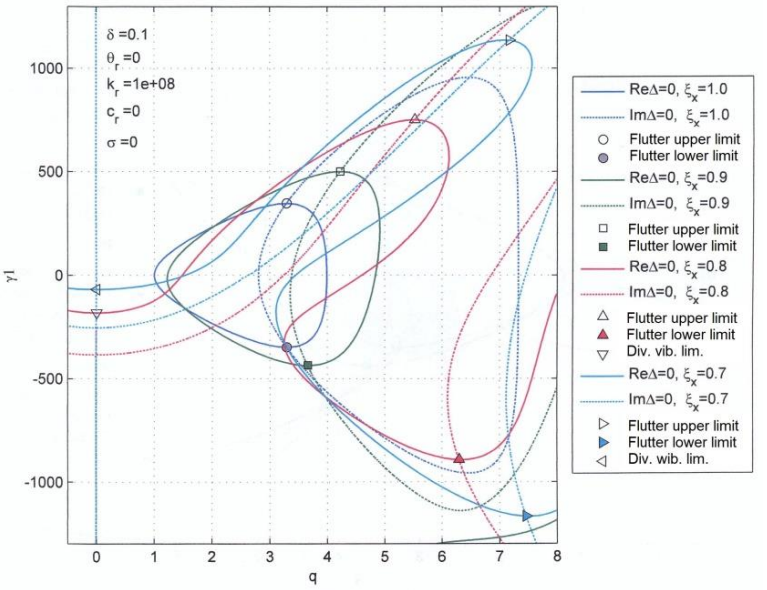

Fig. 3.1. Plots ReΔ = 0 and ImΔ = 0 at $\sigma = 0$ and ξ_x = var

The plots in the foregoing figures were charted for dimensionless parameters of flow $\delta = 0.1$, $\Theta_r = 0$, and support $k_r = 1 \cdot 10^8$, $c_r = 0$, which was infinitely rigid in this case. The characteristic points of intersection of plots ReΔ = 0 and ImΔ = 0 are detailed in the key to the figures. The essence of the figures was to demonstrate the effect of the plate overhang, i.e. $\xi_x < 1$, on the critical parameters of the system in both directions of flow shown in Fig. 1.1.

A preliminary analysis of the figures revealed that plots ReΔ = 0 became desymmetrised, whereas at higher values of the overhang, plot ReΔ = 0 assumed a more complex form on plane γ_1 - q , with e.g. the lower divergence limit gone with the negative sense of flow, i.e. $\gamma_1 < 0$.

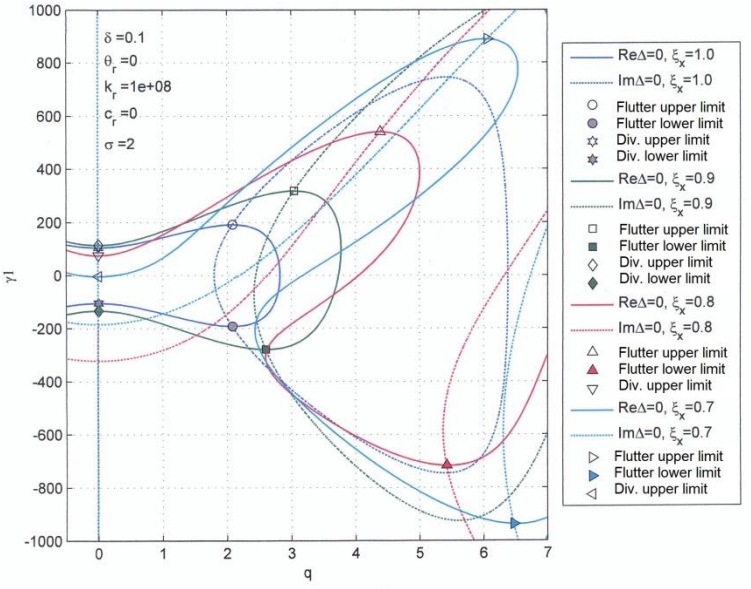

Fig. 3.2. Plots ReΔ = 0 and ImΔ = 0at σ = 2 and σ = 0

The critical parameters of self-excited vibrations and divergence plotted in Figs. 3.1 and 3.2 are listed in Table 3.1.

Table 3.1.

σ	ξ_x	Flutter limit				Divergence limit	
		upper		lower		upper	lower
		q_{kr}	γ_{1kr}	q_{kr}	γ_{1kr}	γ_{1kr}	γ_{1kr}
0	1.0	3.24449	347.459	3.29449	-347.459	-----	----
	0.9	4.22789	500.692	3.65988	-435.699	-----	----
	0.8	5.52657	753.285	6.29635	-892.323	-----	-182.993
	0.7	7.16682	1136.14	7.46485	-1166.61	-----	-69.3533
2	1.0	2.08332	191.732	2.08332	-1191.73	105.641	-105.641
	0.9	3.04352	317.548	2.60256	-278.20	114.673	-133.958
	0.8	4.38985	540.609	5.42368	-716.327	75.536	----
	0.7	6.06551	889.009	6.47705	-937.411	-3.557	----

The following figure, 3.3, illustrates the calculation results for the stable and unstable vibration areas and the flutter and divergence limits in plane $q - \gamma_1$. The calculations were completed for the plate with an overhang of 0.1L, i.e., following the notation from Fig. 1.1, the assumptions were $\xi_x = 0.9$, $k_r = 10^8$, $c_r = 0$. Other parameters not denoted in the plane of the figure were: $\delta = 0.1$, $\Theta_r = 0$.

A reference of the resulting solution to the universal results in [9] from the testing of a plate without any overhang, the foremost conclusion was that no discernible differences in quality were found. The divergence limit plots formed a closed oval form, as before, which was slightly desymmetrised against axis $\gamma_1 = 0$, not unlike the flutter upper and lower limits. For unstable self-excited vibrations, the calculations were completed at $\varepsilon > 0$, and the area of unstable self-excited vibrations was thus determined.

Further on, the forms of vibration at the stability limits were determined at the characteristic points (1) and (2) shown in Fig. 3.3 for both directions of flow (shown with the arrow on the same figure) and for dimensionless parameter $\tau = qt/2\pi$ (Figs. 3.4 and 3.5).

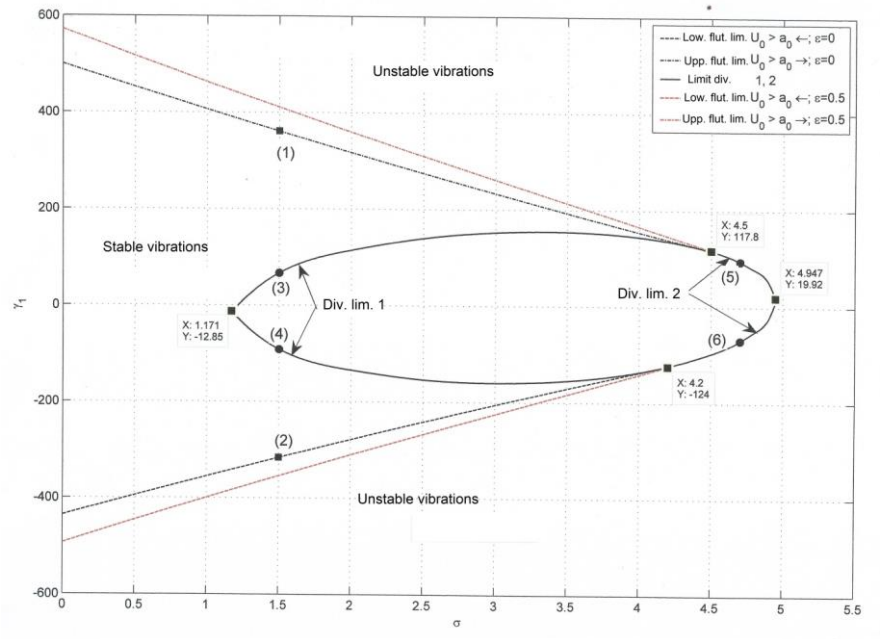

Fig. 3.3. Plate stability limits on plane $\sigma - \gamma_1$
$\left(\xi_x = 0.9, k_r = 10^8, c_r = 0, \delta = 0.1, \theta_r = 0\right)$

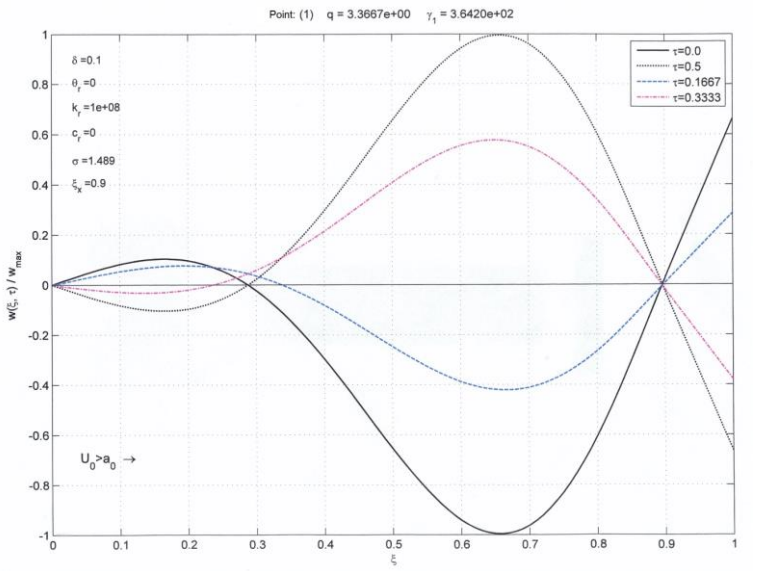

Fig. 3.4. Forms of vibration for the plate with a single moving node (→)

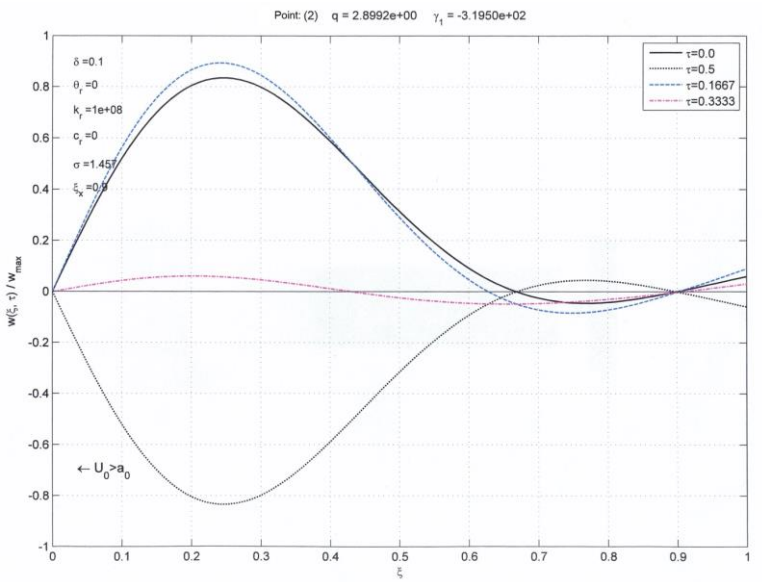

Fig. 3.5. Forms of vibration for the plate with a single moving node (←)

3.2. Determination of the critical parameters of the plate on a fixed hinged support with a moderate overhang ($\xi_x = 0.8$)

The next step of the numerical tests was to determine the effect of the plate overhang size while assuming infinite rigidity of the plate support, $k_r = 10^8$, and two plate overhang values, $\xi_x = 0.8$ and $\xi_x = 0.9$.

The solutions are illustrated in Fig. 3.6, which demonstrates their significant change from the solution to $\xi_x = 0.8$. At higher plate overhang values, the divergence limit ceased to form a closed, oval-like curve and became an open curve with the origin on axis $\sigma = 0$. The characteristic points along the curve are the tangential points of the flutter limit plots with a positive sense of flow ($\sigma = 5.683$; $\gamma_1 = 197.2$) and a negative sense of flow ($\sigma = 8.2$; $\gamma_1 = -451.4$), and two extreme (and reflexive) points with the values ($\sigma = 6.414$; $\gamma_1 = 72.49$) and ($\sigma = 4.094$; $\gamma_1 = -269.4$), respectively. The same figure shows marked areas of stable and unstable vibrations, with a selection of 16 characteristic points for which the forms of vibration and the forms of divergent stability loss were determined.

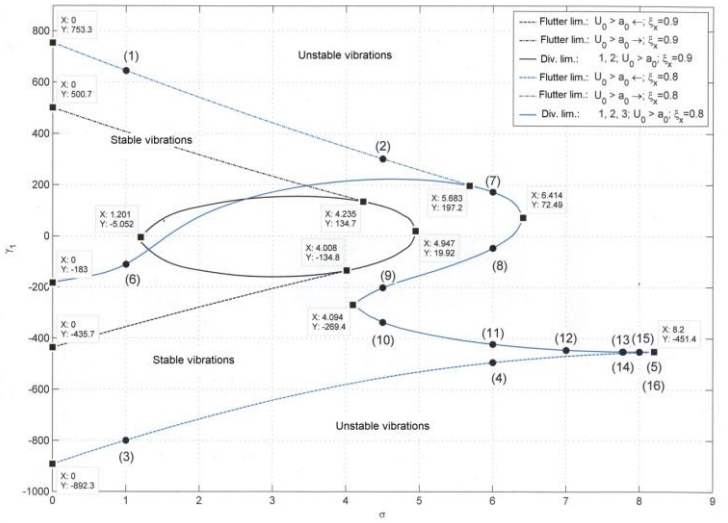

Fig. 3.6. Plate stability limits on plane $\sigma - \gamma_1$
$\left(\xi_x = 0.8, \xi_x = 0.9, k_r = 10^8, c_r = 0, \delta = 0.1, \theta_r = 0\right)$

The charts for points (2) and (4) aligned with the flutter limit are shown in Figs. 3.7 and 3.8, respectively. The parameters for which these plots were charted are shown in the planes of the same figures and in the keys; the important notes resulting from the trends of the plots are listed below the respective figures.

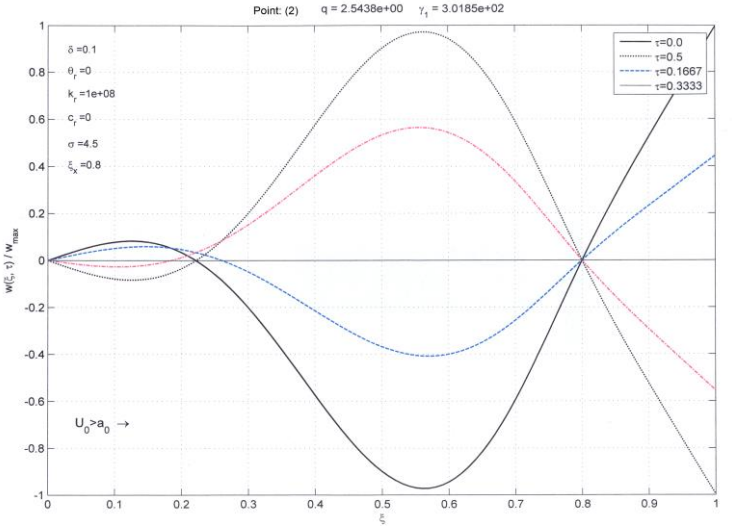

Fig. 3.7. Form of vibration for the plate with a single moving node (point (2))

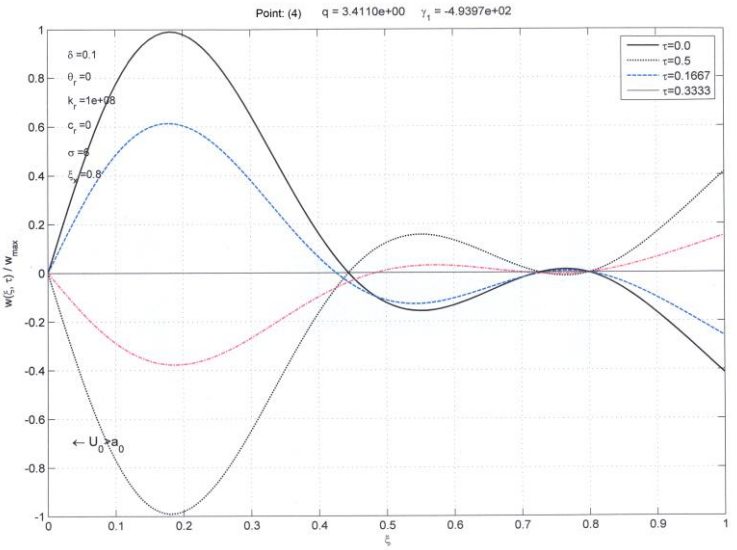

Fig. 3.8. Form of vibration for the plate with two nodes (point (4))

The following figure, 3.9, shows a summary of the trends of divergent stability loss for a selection of characteristic points, (6) to (16), which were positioned in detail in Fig. 3.6. The key and description of the figure detail the parameters assumed for their numerical calculations.

The trends of the plots, and more precisely the number of corresponding node points, determined the type of divergent stability loss in the cases investigated from divergence 1 to divergence 3 (see details in the key to Fig. 3.9).

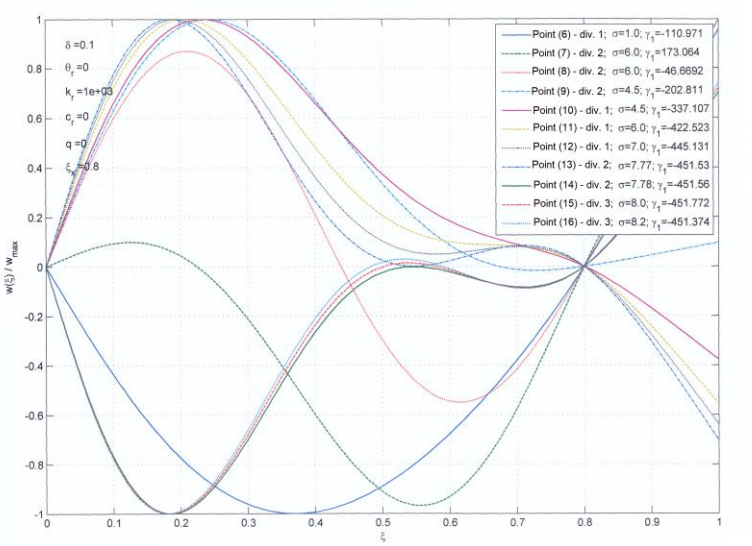

Fig. 3.9. Forms of divergent stability loss of the plate (points (6) to (16))

3.3. Determination of the critical parameters of the plate on a moving flexible hinged support with a moderate overhang ($\xi_x = 0.8$)

Traditionally, determination of the critical parameters comprised charting the plots of $\mathrm{Re}\Delta = 0$ on $\mathrm{Im}\Delta = 0$ plane $q - \gamma_1$ for the determined parameters of the systems and the variable dimensionless value of follower force σ with the determination of the zero points of the characteristic determinant, Δ. In compliance with the procedure set forth herein, areas of stable and unstable vibrations were plotted for infinite and finite rigidity of support, by sequentially assuming $k_r = 10^8$ and $k_r = 10^3$. The results are illustrated in Fig. 3.10.

An analysis of the solution confirmed a known fact from [9] by which the reduction of the support rigidity increased the external area of unstable vibrations. A novel phenomenon was the emergence of an internal area of unstable vibrations (see broken plot lines) in Fig. 3.10. The trends of the flutter limits were determined for the positive value of $\varepsilon = 0.3$ of complex frequency q.

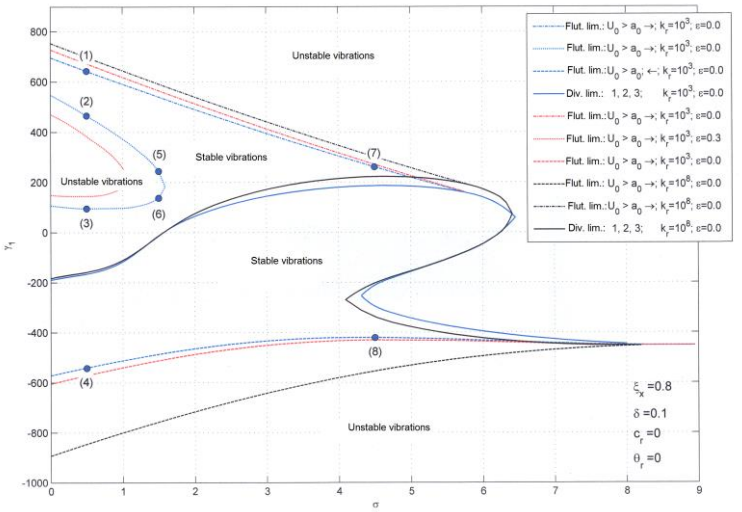

Fig. 3.10. Areas of plate stability on the flexible hinged support with a moderate overhang, with the points shown at which the form of vibration trends were determined

The characteristic points (2), (3) and (8) shown in Fig. 3.10 corresponded to the following forms of vibration.

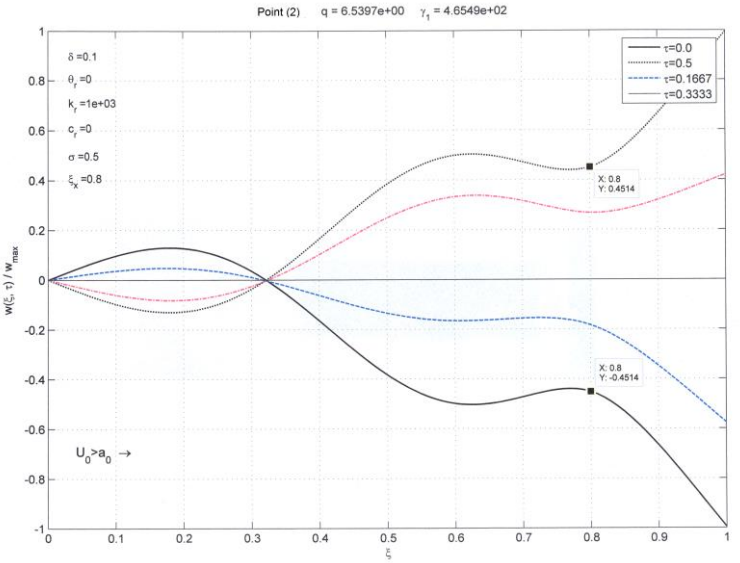

Fig. 3.11. Form of vibration for the plate with a stationary internal node (point (2))

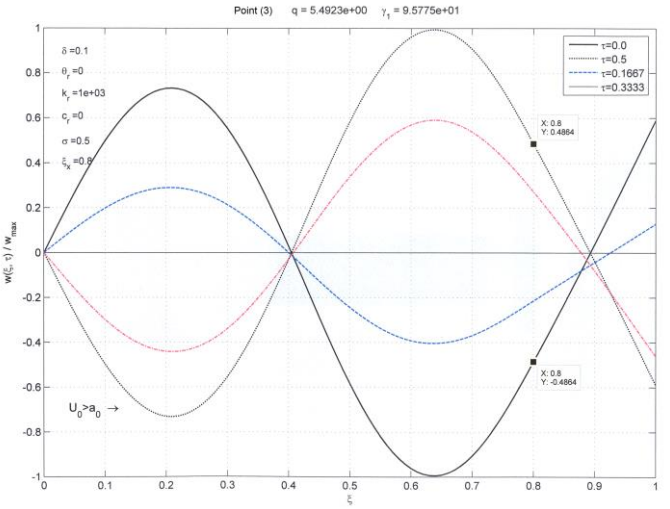

Fig. 3.12. Form of vibration for the plate with two nodes: one internal and nearly stationary, and one external and evidently moving (point (3))

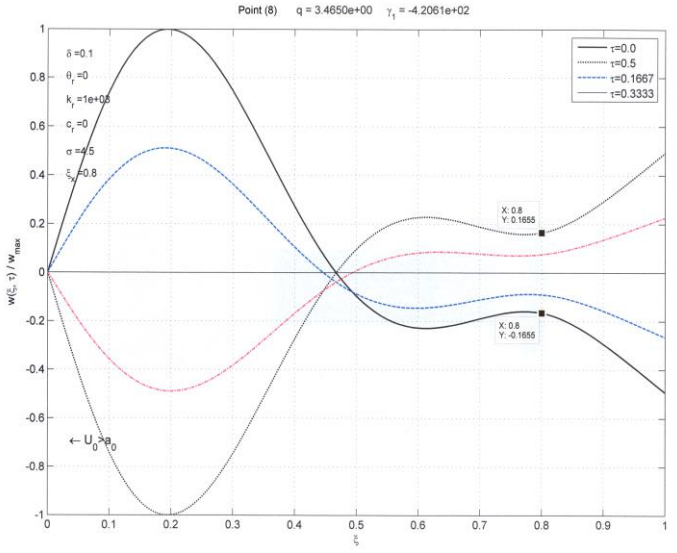

Fig. 3.13. Form of vibrations for the plate with one internal and evidently moving node (point (8))

A common characteristic of all forms of vibration shown so far was the displacement on the resilient support and the significant effect of the direction of flow on the form of deformation shown herein.

3.4. Determination of the critical parameters of the plate on a moving flexible hinged support with a moderate overhang (ξ_x = 0.8) at a change of material attenuation, Θ_r, and aerodynamic attenuation, δ

The first case considered included the effect of material attenuation Θ_r on the locations of stable and unstable vibration areas (Fig. 3.14). An analysis of the effect suggested that material attenuation increased the unstable vibration areas while the character of the solution was retained. The calculation input parameters and a detailed description thereof is shown in the figure plane and key. The second case considered concerned the effect of aerodynamic attenuation δ on the locations of stable and unstable vibration areas (Fig. 3.15). Here, the unstable vibration areas also grew while the character of the solution was retained while aerodynamic attenuation grew. The calculation input parameters and a detailed description thereof is shown in the figure plane and key.

A general note should be made that both attenuation types for the plate with no overhang (see [9]) and the plate with the overhang led to the same quantitative conclusions. With the moderate and higher overhangs, i.e. $\xi_x \leq 0.8$, the quantitative nature of the solution was quite different. Two new phenomena were revealed; first, the internal separation of the divergent stability loss limit oval into a single plot line with the origin at axis $\sigma = 0$; second, the emergence of a stable internal area of unstable vibrations.

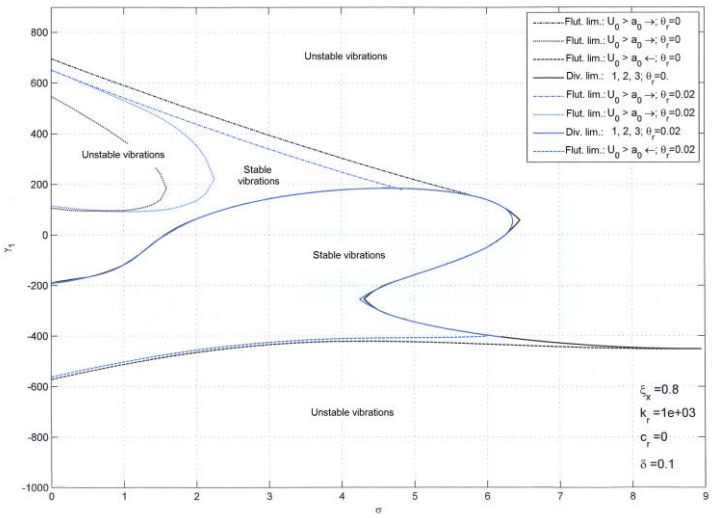

Fig. 3.14. Areas of stable and unstable vibration with the change in material attenuation Θ_r

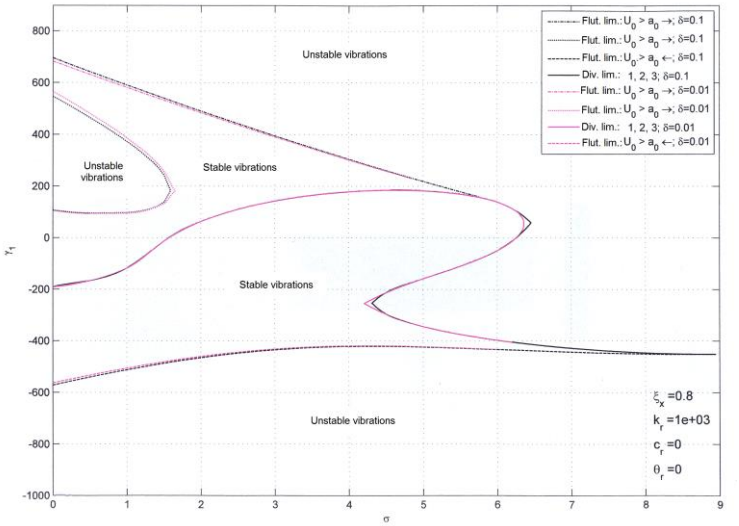

Fig. 3.15. Areas of stable and unstable vibration with the change in aerodynamic attenuation δ

4. CONCLUSION FOR THE TEST RESULTS

The analysis completed as contemplated herein determined the characteristics of the vibrations and stability of a plate with a finite overhang exposed to a supersonic flow and investigated as a double self-excited system, in which two independent physical factors occurred that triggered the self-excitation phenomenon: the supersonic flow and the compressive follower force applied in the plate plane. Two directions of supersonic flow were considered with an assumption that one of the plate edges was on a hinged support, while the other featured a resilient support which assumed different positions along the plate length, L.

The limits of the system's vibration stability areas were analysed in plane (σ, γ_1), with γ_1 being a dimensionless parameter determining the dynamic pressure of the gas flow acting on the vibrating panel, and σ being the dimensionless compressive follower force acting within the plate plane. The analysis suggested that within that plane, without overhang L - L_x = 0 or with a low overhang, L - L_x = 0.1, an oval occurred, which defined the divergence limits of the first two natural vibrations of the system in both directions of flow, and the plot lines connected to the oval and describing the limits of self-excited vibration areas at $\gamma_1 \geq 0$ and $\gamma_1 \leq 0$, i.e. for both directions of flow. The solutions obtained for L_x = 0.9 (the plate with a minimum overhang) and for L_x = 1 (the plate with no overhang) feature very little qualitative and qualitative differences.

In [9] features a series of numerical calculations for $L_x = 1$ were carried out. The results demonstrated how the said ovals and self-excited vibration limits changed in relation to the plate support method and other parameters of the problem, and thus, they do not require a detailed discussion. The focus hereof included the numerical test results with $L_x \leq 0.8$. In this case, $L_x = 0.8$, it was found that: (I) the inner oval was divided, with its upper part joining the plot axis $\sigma = 0$, whereas its lower part, when at high values of σ, which were $\sigma = 9$ here, became tangent with the lower plot of the self-excited vibration area limit; (II) two inner areas of unstable vibrations emerged, with the upper one stable and the lower one symmetrical to axis $\gamma_1 = 0$ and unstable (and only theoretically feasible), and with $\Theta_r \neq 0$, it would not exist. Aside from the rigidity of the right-hand resilient support, a major contributor to the locations of the stability limits of the system was the values of coefficients of aerodynamic attenuation δ, material attenuation Θ_r, and the attenuation within the resilient support c_r. It was determined that an increase in aerodynamic attenuation (Fig. 3.15) stabilised the system, while material attenuation (Fig. 3.14) and the attenuation within the resilient support contributed to instability.

REFERENCES

[1] Bisplinghoff L. Raymond, Holt Ashley. 1962. *Principles of Aeroelasticity*. New York: John Wiley.

[2] Dżygadło Zbigniew. 1969. "On nonautonomous boundary value problems of pates oscillating in supersonic flow". *Fluid Dynamics Transactions*, v. 4.

[3] Dżygadło Zbigniew, Lech Solarz. 1970. "On nonautonomous vibrations of a self- excited system with tangential force". *Proceedings of Vibration Problems* 11(2).

[4] Dżygadło Zbigniew, Adam Krzyżanowski. 1972. "Self-excited and forced vibrations of an aeroelastic system subject to a follower force". *Proceedings of Vibration Problems* 13(3).

[5] Dżygadło Zbigniew, Idzi Nowotarski, Aleksander Olejnik. 1976. "Analysis of self-excited and forced vibrations of a cylindrical shell in supersonic flow". *Jour. of Tech. Phys.* 17(1).

[6] Bogusz Władysław, Zbigniew Dżygadło, Dominik Rogula, Kazimierz Sobczyk, Lech Solarz. 1992. *Vibrations*. Warsaw: PWN

[7] Higuchi K., E.H. Dowell. 1992. "Effect of structural damping on flutter of plates with a follower force". *AIAA Journal* 30(3) : 820-825.

[8] Lien-Wen Chen, Der-Ming Ku. 1992. "Stability of elastic systems under follower forces". *AIAA Journal* 30(3) : 767-771.

[9] Dżygadło Zbigniew, Idzi Nowotarski, Aleksander Olejnik. 1998. "Drgania i stateczność płyty w opływie naddźwiękowym obciążonej siłą śledzącą". *Prace Instytutu Lotnictwa* 155(4)

Drgania i stateczność płyty w opływie naddźwiękowym obciążonej siłą śledzącą z przegubową podporą zewnętrzną i wewnętrzną sprężysto-tłumiącą

Idzi NOWOTARSKI

Wydział Mechatroniki i Lotnictwa, Wojskowa Akademia Techniczna
ul. gen. Witolda Urbanowicza 2, 00-908 Warszawa

Streszczenie. Rozpatrzono drgania i stateczność płyty o skończonej długości w płaskim przepływie naddźwiękowym przy założeniu, że jedna z krawędzi płyty jest przegubowo podparta, a druga jest swobodna. W wewnętrznym punkcie płyty znajduje się podpora o własnościach sprężysto-tłumiących. W płaszczyźnie płyty działa siła ściskająca, która jest siłą śledzącą i zachowuje kierunek styczny do odkształconej powierzchni płyty. Powstaje w ten sposób układ powierzchniowy, w którym występują dwa niezależne czynniki fizyczne będące przyczyną jego samowzbudności. Jest to więc układ, który można nazwać układem podwójnie samowzbudnym. Rozwiązanie równań ruchu otrzymano za pomocą przekształcenia Laplace'a. W dalszej części pracy przeprowadzono numeryczną analizę warunków występowania samowzbudnych drgań w zależności od położenia podpory wewnętrznej (tzw. przewieszenia płyty), tłumienia w materiale płyty oraz innych jej parametrów, w tym także parametrów sprężysto-tłumiących podpory. Dla przyjętych parametrów zbadano wyniki obliczeń granic obszarów stateczności i niestateczności rozpatrywanego układu na płaszczyźnie γ_1, σ. i wyznaczono postacie drgań dla szeregu typowych przypadków.
Słowa kluczowe: mechanika, aerosprężystość, model matematyczny